SANDIA REPORT

SAND2012-7281
Unlimited Release
Printed August 2012

Calculation of Nucleation Pathways in Membrane Systems

Christina L. Ting and Zhen-Gang Wang

Prepared by
Sandia National Laboratories
Albuquerque, New Mexico 87185 and Livermore, California 94550

Sandia National Laboratories is a multi-program laboratory managed and operated by Sandia Corporation, a wholly owned subsidiary of Lockheed Martin Corporation, for the U.S. Department of Energy's National Nuclear Security Administration under contract DE-AC04-94AL85000.

Approved for public release; further dissemination unlimited.

Sandia National Laboratories

Issued by Sandia National Laboratories, operated for the United States Department of Energy by Sandia Corporation.

NOTICE: This report was prepared as an account of work sponsored by an agency of the United States Government. Neither the United States Government, nor any agency thereof, nor any of their employees, nor any of their contractors, subcontractors, or their employees, make any warranty, express or implied, or assume any legal liability or responsibility for the accuracy, completeness, or usefulness of any information, apparatus, product, or process disclosed, or represent that its use would not infringe privately owned rights. Reference herein to any specific commercial product, process, or service by trade name, trademark, manufacturer, or otherwise, does not necessarily constitute or imply its endorsement, recommendation, or favoring by the United States Government, any agency thereof, or any of their contractors or subcontractors. The views and opinions expressed herein do not necessarily state or reflect those of the United States Government, any agency thereof, or any of their contractors.

Printed in the United States of America. This report has been reproduced directly from the best available copy.

Available to DOE and DOE contractors from
U.S. Department of Energy
Office of Scientific and Technical Information
P.O. Box 62
Oak Ridge, TN 37831

Telephone: (865) 576-8401
Facsimile: (865) 576-5728
E-Mail: reports@adonis.osti.gov
Online ordering: http://www.osti.gov/bridge

Available to the public from
U.S. Department of Commerce
National Technical Information Service
5285 Port Royal Rd
Springfield, VA 22161

Telephone: (800) 553-6847
Facsimile: (703) 605-6900
E-Mail: orders@ntis.fedworld.gov
Online ordering: http://www.ntis.gov/help/ordermethods.asp?loc=7-4-0#online

SAND2012-7281
Unlimited Release
Printed August 2012

Calculation of Nucleation Pathways in Membrane Systems

Christina L. Ting
Biochemistry and Molecular Biophysics
California Institute of Technology
Pasadena, California 91125

Zhen-Gang Wang
Chemical Engineering
California Institute of Technology
Pasadena, California 91125

Abstract

Within self-consistent field theory, we develop an "on-the-fly" string method to compute the minimum free energy path for several activated processes involving a charged, solvophobic nanoparticle and a lipid membrane. Under tensions well below the mechanical stability limit of the membrane, and in the regime where nucleation can occur on experimentally relevant time scales, our study suggests that there can be at least three competing pathways for crossing the membrane: (1) particle-assisted membrane rupture, (2) particle insertion into a metastable pore followed by translocation and membrane resealing, and (3) particle insertion into a metastable pore followed by membrane rupture. In the context of polymer-based gene delivery systems, this suggests a novel role of the particle in the endosomal escape, not previously envisioned in the proton sponge hypothesis. The methodology developed in this work represents the most advanced theoretical technique for describing nucleation pathways in soft condensed matter systems that also include hard-particle degrees of freedom.

Acknowledgment

The authors wish to thank Daniel Appelö for many helpful discussions. This work was supported by the Joseph J. Jacobs Institute for Molecular Engineering for Medicine and by a Sandia Campus Executive LDRD to C.L.T. The computing facility on which the calculations were performed is supported by an NSF-MRI grant, Award No. CHE-1040558.

Contents

1 Introduction **9**

2 Model and Method **11**

3 Results **15**

4 Conclusion **21**

References **23**

List of Figures

3.1 Density plots of the transition states for homogeneous rupture 15

3.2 Density plots along the MFEP for rupture with particle when $\gamma = 0.6$. 16

3.3 Free energy profile of the MFEP for rupture with particle 17

3.4 Density plots along the MFEP for rupture with particle when $\gamma = 1.9$ 17

3.5 Free energy profile of the MFEP for particle translocation 18

List of Tables

2.1 Parameters used for the model membrane 12

Chapter 1

Introduction

The interaction of nanoparticles with lipid membranes is a common theme underlying a number of important topics in bionanotechnology, ranging from cytotoxicity [1] to the delivery of therapeutics [2]. In polymer-based gene delivery systems [3], the nanoparticle is comprised of genetic material condensed with cationic polymers. Once internalized by the cell via endocytosis, the nanoparticles are enclosed within membrane-bound vesicles called endosomes, and are trafficked along the endolysosomal pathway, where acidification activates hydrolytic enzymes [4]. Hence, the nanoparticle must escape the endosome before crossing the nuclear envelope for successful gene expression. Clearly, membrane-particle interactions play a central role in several key steps along the gene delivery pathway. In particular, understanding the endosomal escape mechanism provides a direct motivation for the work described in this report.

In the proton-sponge hypothesis [5–7], the nanoparticle plays an *indirect* role in its own endosomal escape by serving as a buffering substrate for protons. As additional protons are pumped into the endosome with an attendant influx of counterions, the increase in osmotic pressure translates to increased tension on the endosomal membrane. Eventually the membrane ruptures, thus releasing the trapped nanoparticles into the cytosol. Importantly, membrane rupture is a thermally nucleated process [8–13] under the small to moderate tensions generated in the proton sponge hypothesis [7, 14]. It is therefore possible to imagine that the nanoparticle takes a more *direct* role in the endosomal escape by interacting directly with the membrane to lower the nucleation barrier for rupture. We examine this scenario in the broader context of nucleated pathways involving membrane-particle interactions.

A number of computational studies on membrane-particle systems have been conducted to elucidate the equilibrium structures [15–19], as well as the dynamics under (nearly) spontaneous conditions [20, 21] or when induced by an external force [22]. However, these studies have not addressed the thermally nucleated processes we are interested in here. Besides the long time scales associated with these rare events, a significant challenge arises because of the high dimensional free energy surface due to the conformation degrees of freedom of the lipid molecules, characteristic of many soft matter systems. Hence, with any sizable nucleation barrier, direct computer simulation is unfeasible. The potential of mean constraint force method attempts to overcome this challenge by artificially choosing a reaction coordinate that (in general) does not coincide with the true nucleation pathway, while the transition path sampling method [23, 24] is impractical for systems involving large assemblies of complex molecules.

Recently, two groups [13, 25] have developed a powerful mean-field technique for studying minimum free energy paths (MFEP) in self-assembled polymeric systems. The technique combines the self-consistent field theory (SCFT) [26] with the string method [27, 28], and overcomes the aforemetioned time scale and dimensionality challenges. Ting et al. [13] have applied this technique to study nucleated pore formation and rupture in membrane bilayers. To explore nucleated pathways involving the membrane-nanoparticle interactions of interest here, we must further account for the particle degree of freedom. This highly nontrivial task requires additional development in the methodology. We therefore start with a description of the model and method.

Chapter 2

Model and Method

Our membrane bilayer consists of double-tailed amphiphiles (A) assembled in explicit solvent (S) containing ions ($\pm$). The amphiphiles are modeled as discrete Gaussian chains having a solvophilic head (H) segment of N_H negatively charged monomers with volume v_H and two solvophobic tail (T) segments, each consisting of N_T monomers with volume v_T. The solvents are modeled as monomers with volume v_S and the ions are represented as monovalent point charges of the elementary charge e. The short-ranged repulsion involving the monomer units is represented by an incompressibility condition everywhere in the system. We work in the grand canonical ensemble, where the number of molecules are determined from their respective chemical potentials μ_J ($J = A, S, \pm$). In addition to the fluid species, there is a positively charged nanoparticle (P), whose density profile is defined by a cavity function that excludes the fluid species from its interior:

$$h_P(|\mathbf{r}-\mathbf{r}_P|) = \frac{1}{2}\left(1+\tanh[(R_P-|\mathbf{r}-\mathbf{r}_P|)/w]\right). \tag{2.1}$$

Here, R_P is the particle radius, w is the width of the interface and $\mathbf{r}_P$ is the particle position [29,30].

The essential contributions to the model are the chain connectivity of the amphiphiles, the incompressibility condition, the short-ranged pairwise interactions and the long-ranged electrostatic interactions. The derivation of the SCFT is described in detail in Refs. [13, 18, 26]. The final expression for the grand potential is:

$$\begin{aligned} F = &-\frac{e^{\mu_A}}{v_A} Z_A[\xi_H,\xi_T] - \frac{e^{\mu_S}}{v_S} Z_S[\xi_S] - \frac{e^{\mu_\pm}}{v_\pm} Z_\pm[\psi] \\ &+ \int d\mathbf{r} \left\{ \sum_{JK} \left[\chi_{JK}\phi_J\phi_K + \frac{\kappa_J}{2}|\nabla\phi_J|^2 - \xi_J\phi_J \right] + \chi_{TP}\phi_T h_P + \psi\rho_c - \frac{\varepsilon}{2}|\nabla\psi|^2 \right\}. \end{aligned} \tag{2.2}$$

Here the summation is over $JK \in \{HT, TS, SH\}$ and the fields ϕ_J, ξ_J, and ψ denote the monomer volume fraction, its conjugate potential, and the electrostatic potential fields, respectively. For notational conciseness we omit the $\mathbf{r}$ dependence in these field variables. The partition functions in the first line account for the Boltzmann weight of a single molecule in its respective field(s), and are given by

$$\begin{aligned} Z_A[\xi_H,\xi_T] &= \int d\mathbf{r} q_H(\mathbf{r},N_H) e^{2v_H\xi_H} q_T^2(\mathbf{r},N_T+1), \\ Z_S[\xi_S] &= \int d\mathbf{r} \exp\{-v_S\xi_S\}, \\ Z_\pm[\psi] &= \int d\mathbf{r} \exp\{\mp\psi e - u_\pm^b\}, \end{aligned} \tag{2.3}$$

i	v_i	N_i	ε_i	κ_i	χ_{iH}	χ_{iT}	χ_{iS}
H	0.05	5	50	0	—	75	—
T	0.05	10	2	8	—	—	22
S	0.15	1	80	0	0	—	—

Table 2.1. (L to R) The monomer volume, number of monomers, dielectric value [33], gradient coefficient, and Flory parameters. $c_\pm = 100$ mM for the bulk ion concentration.

for the amphiphiles, solvents, and ions, respectively. Here q_H and q_T are the chain propagators used to obtain the single-chain statistics for each arm of the amphiphile [18].

$$u_\pm^b = e^2(8\pi a_\pm \varepsilon)^{-1} \tag{2.4}$$

is the Born self-energy of an ion, where ε is the spatially varying dielectric constant (assumed to be a simple local volume-fraction weighted average) and $a_\pm = 0.1$ nm is the Born radius.

In Eq. (2.2), the local and non-local parts of the pairwise interactions are captured by χ_{JK} and κ_J, respectively [31]. Their values (see Table 2.1) are chosen to reproduce some known experimental properties of lipid membranes; in particular, the linear stretching modulus for our model is found to be 210 mN/m [32]. The solvophobicity of the nanoparticle is modeled by a Flory-like parameter χ_{TP} that acts locally over the interfacial region of the particle and the total fixed charge density is defined $\rho_c = c_P h_P + (c_H/v_H)\phi_H$. Here c_P is the charge density on the nanoparticle and $c_H = -0.05$ is the charge per head monomer. The SCF equations are obtained by requiring that Eq. (2.2) be stationary with respect to variations in the fields, i.e. $\frac{\partial F}{\partial \omega}|_{\omega^*} = 0$, where $\omega = \phi_I, \xi_I, \psi$. These equations are then solved iteratively until convergence, with the solutions corresponding to (meta)stable equilibrium states of the system.

However, our interest here is in the nucleation pathways between equilibrium states, and in particular the transition state, i.e. the critical nucleus. To map out these pathways, which necessarily include nonequilibrium states, we apply the string method to Eq. (2.2). Briefly, we begin with a string of discrete states in the space defined by the density fields of the monomer species and the nanoparticle. The string is relaxed towards the MFEP by a two-step iterative procedure: (1) an evolution equation describing the steepest descent dynamics on the free energy landscape and (2) a redistribution of the states along the string. The latter step is key, as it prevents all the states from falling into one of the trivial equilibrium solutions. While the string method is easily implemented on a known free energy landscape, in SCFT the free energy as a functional of the densities is not known *a priori*. Thus we take an "on the fly" approach to traverse the free energy landscape by evaluating the gradients of Eq. (2.2) using a combination of the external potential dynamics (EPD) [34] and hybrid particle field (HPF) [29] methods.

More specifically, we first evolve the states for some time Δt according to the steepest descent dynamics of the density fields. This approach is similar to that taken in dynamic SCFT [35], but for computational convenience (see also Ceniceros and Fredrickson [36] for the target density

problem), we choose to reformulate the dynamics in terms of the fields ξ_I, using the EPD method:

$$\frac{\partial \xi_I}{\partial t} = D_1 \frac{\delta F}{\delta \phi_I}. \tag{2.5}$$

Here D_1 is a scalar mobility coefficient and $\delta F/\delta\phi_I$ is the familiar functional derivative of Eq. (2.2) so that ξ_I is updated by simple time iteration methods [37]. ϕ_I follows as usual by solving the modified diffusion equation for the chain propagators in the presence of the new ξ_I [18]. Next, we evolve the particle position $\mathbf{r}_P$ according to the HPF method developed by Sides et al. [29]:

$$\frac{\partial \mathbf{r}_P}{\partial t} = -D_2 \frac{\partial F}{\partial \mathbf{r}_P} = -D_2 \frac{\delta F}{\delta h_P} \mathbf{g}(\mathbf{r_p} - \mathbf{r}), \tag{2.6}$$

where $\mathbf{g}(\mathbf{r}) \equiv \frac{1}{r}\frac{dh_P(r)}{dr}\mathbf{r}$ is a vector function related to the derivative of the cavity function. The density fields and the particle position are then updated, subject to the incompressibility condition.

The second step in the string method involves a redistribution of the states along the string. In the simplest case, this is enforced by an equal arc-length reparametrization of the string based on the current densities, followed by a linear interpolation to obtain the new densities. The two dynamical equations [Eq. (2.5) and Eq. (2.6)], followed by the reparametrization, are computed at every time step. Once converged, the string coincides with the MFEP. In what follows, we discuss the main results.

Chapter 3

Results

To understand the effect of the nanoparticle on membrane pore formation and rupture, we first consider the case in the absence of the nanoparticle, i.e. homogeneous rupture. The free energy barrier F_0^* diverges for a tensionless membrane and vanishes at a threshold tension γ_t = 5.1, corresponding to the onset of mechanical instability. The structure and free energy of the transition state in the intermediate regime will depend on the membrane tension. For low tensions ($\gamma = 0.6$) the transition state corresponds to a well-defined pore with $F_0^* = 75$, whereas for higher tensions ($\gamma = 1.9$) the transition state corresponds to a solvophilic stalk with $F_0^* = 24$; see Fig. 3.1. Assuming an Arrhenius rate expression of the form $k = \nu \exp[\ \ F^*]$, where $\nu \sim 10\ \mu$s is a transition frequency associated with the molecular relaxation [38], nucleation will take place on experimentally relevant time scales if $F^* \lesssim 25$. Thus, nucleation is a relevant mechanism for homogeneous rupture of a membrane under moderate tensions ($\gamma \gtrsim 1.9$).

Next, we proceed to examine the effect of a charged and/or solvophobic nanoparticle on the nucleation barrier to rupture, beginning with the low tension case ($\gamma = 0.6$). The string is initialized between two fixed end states [see Fig. 3.2(a) and (f)] and evolved according to the algorithms described earlier. The resulting MFEP reveals the following nucleation pathway. Through electrostatic attraction, the positively charged particle adsorbs onto the surface of the negatively charged membrane. This metastable state is shown in (b). From here, rupture takes place by a two-step nucleation process. First, the particle pushes into and punctures the membrane, overcoming the first barrier; see (c). Note that the trans leaflet, which is already thinned in (b), is broken first and the

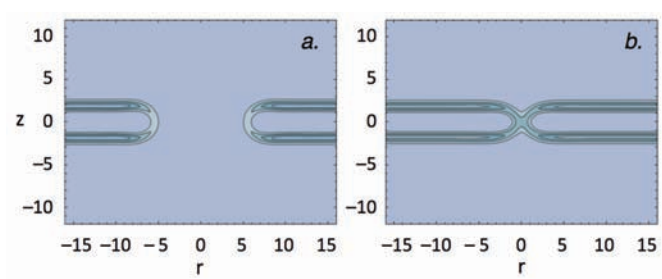

Figure 3.1. The transition state for homogeneous membrane rupture when $\gamma = 0.6$ (*a*) and $\gamma = 1.9$ (*b*). Contour plots show the lipid head densities in cylindrical coordinates.

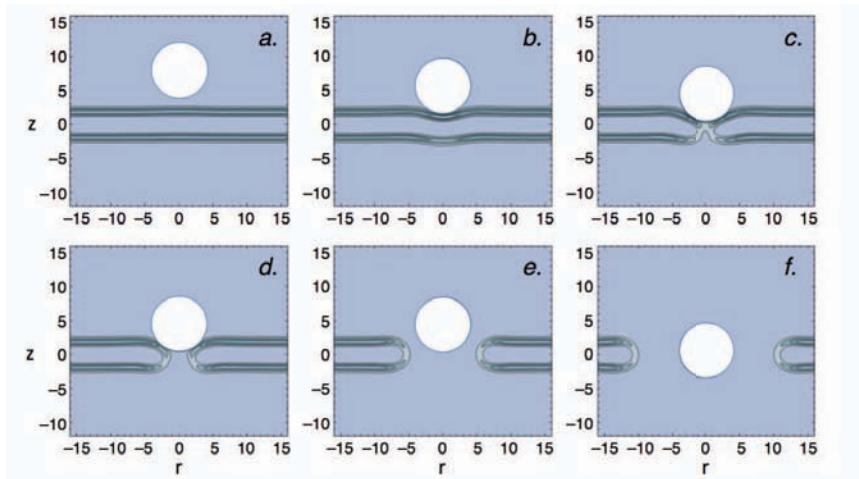

Figure 3.2. Membrane under low tension ($\gamma = 0.6$): states along the MFEP for membrane rupture in the presence of a nanoparticle ($R_P = 4$, $c_P = 0.5$, $\chi_{TP} = 0$).

cis leaflet is held intact by the electrostatic attraction to the particle. Once the membrane bilayer is broken, the particle sits in a highly transient metastable pore that is lined by lipid head groups, as shown in (d). From here the membrane can expel the particle and reseal the defect. However to proceed to rupture, the pore must expand to some critical radius r^*; see (e). Importantly, $r^* > R_P$ for this case and hence the second transition state in the two-step nucleation pathway is essentially the same as the transition state for homogeneous rupture; compare (e) with Fig. 3.1(a).

In Fig. 3.3, the MFEP for rupture in the presence of a particle is plotted as a function of the true reaction coordinate s that defines the set of images along the string, and also as a function of the particle position z, for several values of membrane tension. In all cases, the charged nanoparticle first adsorbs onto the surface of the membrane, stabilizing the initial state. For the low tension case ($\gamma = 0.6$), rupture then proceeds by the two barrier crossings described above: puncturing the membrane with rate k_1 [Fig. 3.2(c)] and expanding the pore with rate k_2 [Fig. 3.2(e)]. The first of these is reversible, with backward rate k_{-1}, and the second, irreversible. Intermediate to the two transition states is the transient, metastable pore [Fig. 3.2(d)]. The mean first-passage time for this two-step nucleation process is given by

$$\tau = \frac{1}{k_1} + \frac{k_{-1}}{k_1 k_2} + \frac{1}{k_2}, \tag{3.1}$$

and the nucleation rate may be approximated as $J = \tau^{-1}$ [39,40]. Here, breaking the surface of the membrane is the more energetically costly step, with $F_1^* = 51$. Furthermore, because the reverse rate k_{-1} for the transient state to expel the particle and reseal the pore is high ($F^*_{-1} = 3$, whereas $F_2^* = 45$), rupture can effectively be considered crossing a single barrier with $F^* = 93$. Recall $F_0^* = 75$ for homogenous rupture; thus, for a membrane under low tension the particle does not assist in rupture.

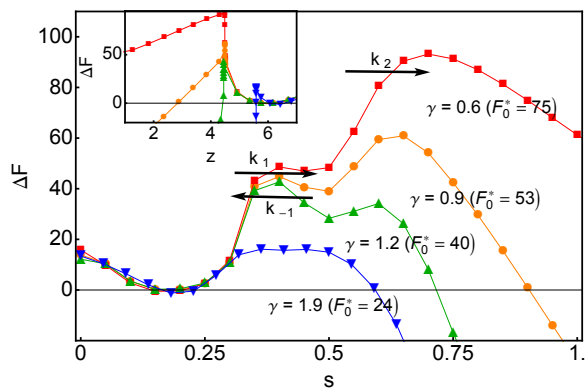

Figure 3.3. The MFEP for membrane rupture in the presence of a nanoparticle ($R_P = 4$, $c_P = 0.5$, $\chi_{TP} = 0$), as a function of the reaction coordinate s and the particle position z (inset) for several values of tension. The nucleation barrier for homogeneous rupture is shown in parentheses.

In the proton sponge hypothesis, the membrane tension is believed to play an important role in the endosomal escape [7]. We find that with increasing tension, the metastable pore becomes more stable with respect to resealing k_{-1} but less stable with respect to rupture k_2, and eventually unstable altogether; see Fig. 3.3. In particular, for $\gamma = 1.9$ rupture becomes a one-step nucleation process. To understand this result, recall that for this tension the transition state for homogeneous rupture is a solvophilic stalk with $F_0^* = 24$ [Fig. 3.1(b)]. The transition state for particle-assisted membrane rupture also corresponds to a solvophilic stalk [Fig. 3.4(c)], but with a reduced barrier $F^* = 18$ (Fig. 3.3). Here the positively charged nanoparticle is able to interact with both leaflets of the membrane to facilitate the formation of the stalk-like structure, thereby lowering the nucleation barrier to rupture. This result suggests a *direct* role of the nanoparticle in the endosomal escape, not previously envisioned in the proton sponge hypothesis, and illustrates the importance of having an induced tension on the membrane.

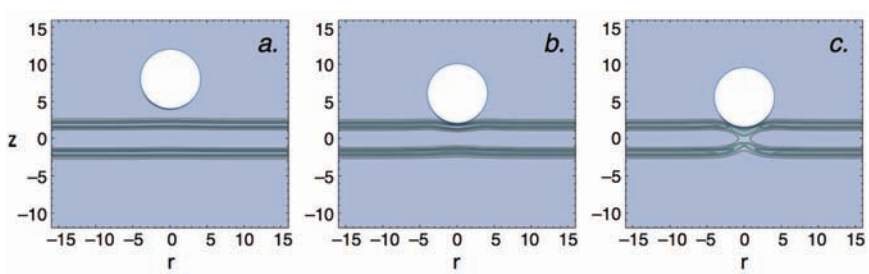

Figure 3.4. Membrane under moderate tension ($\gamma = 1.9$): states along the MFEP for membrane rupture in the presence of a nanoparticle ($R_P = 4$, $c_P = 0.5$, $\chi_{TP} = 0$).

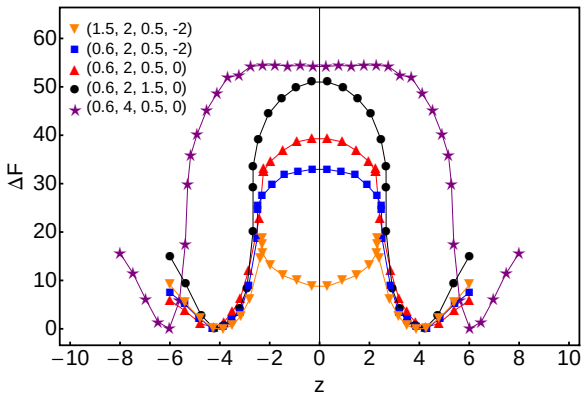

Figure 3.5. The MFEP for particle translocation as a function of the particle position z for different tensions and particle parameters, corresponding to $(\gamma, R_P, c_P, \chi_{TP})$.

Next, we consider particle translocation as an alternate path for the endosomal escape. Here the particle crosses without rupturing the membrane. Beyond the delivery of medical therapeutics, particle translocation is of interest for understanding the mechanisms of nanoparticle cytotoxicity [41] and viral cell entry [42], and is therefore of interest in its own right. We return to the membrane under low tension ($\gamma = 0.6$) and the same particle considered previously. The critical pore radius of the transition state for rupture is larger than the radius of the particle. For successful translocation the particle only needs to create a pore large enough to pass through, and thus we expect translocation to be the preferred pathway over rupture. Although still highly unlikely, translocation is indeed the more favorable mechanism for crossing the membrane, where $F^* = 54$ (Fig. 3.5$\star$).

To lower the barrier to the regime where translocation can occur on experimentally relevant time scales, we consider the effects of the particle size, charge and solvophobicity. Particles smaller than the critical pore radius for homogeneous rupture should translocate more easily. Reducing the particle size to $R_P = 2$ while maintaining the same charge density and solvophobicity, we find that the free energy barrier is indeed lowered to $F^* = 39$ (Fig. 3.5$\triangle$), which is still on the high side for thermally-nucleated translocation. With the reduced particle size, we increase the charge density to $c_P = 1.5$, and find the free energy barrier is *increased* to $F^* = 51$ (Fig. 3.5$\circ$). This result can be rationalized by noting that the density of negatively charged amphiphilic heads is higher for an intact membrane compared to a pore with high curvature. Thus the particle gains more favorable electrostatic interactions by adsorbing onto the surface rather than inserting into a pore. If instead we increase the particle solvophobicity by setting $\chi_{TP} = -2$, the particle is able to interact with the solvophobic tail region of the membrane, thereby *lowering* the free energy barrier for translocation to $F^* = 33$ (Fig. 3.5$\square$).

Based on these results, we find that translocation of a charged and/or solvophobic nanoparticle through a membrane under low tension is unlikely to occur by thermal nucleation. However, particle translocation becomes possible upon increasing the membrane tension. Taking the particle

with the lowest free energy barrier for translocation ($R_P = 2$, $c_P = 0.5$, $\chi_{TP} = -2.0$), we increase the membrane tension to $\gamma = 1.5$ and find that the particle inserted into the middle of the membrane is now a metastable state along the MFEP; see (Fig. 3.5$_{\triangledown}$). Translocation is now a two-step process, the first barrier corresponding to particle insertion, with $F_1^* = 19$, and the second barrier corresponding to expelling the particle and resealing the pore, with $F_2^* = 10$. Using Eq. (3.1), we compute the nucleation rate for translocation and find $J = \nu \exp[-19.6]$, indicating that the process can occur on experimentally relevant time scales.

Interestingly, the critical nucleus for homogeneous rupture in this case is a pore on the order of the size of the particle. Therefore, the electrostatic attraction between the positively charged nanoparticle and the negatively charged amphiphilic heads are able to stabilize the pore, preventing rupture. Based on this result, we can imagine a third pathway for crossing the membrane barrier: particle insertion into the metastable pore followed by rupture. From our MFEP calculation, we find $F_1^* = 19$ and $F_{2'}^* = 8$ for insertion and rupture, respectively, so that the overall nucleation rate for crossing the two barriers is $J = \nu \exp[-19.1]$. Note that in the earlier mechanism depicted in Fig. 3.2 and Fig. 3.3, the metastable state is a partially punctured membrane, whereas here the metastable state is a membrane pore with a fully inserted particle.

Chapter 4

Conclusion

We conclude with some general remarks on nucleated pathways for a nanoparticle to cross the bilayer membrane, and some implications for the endosomal escape in gene delivery systems. Our results indicate at least three competing pathways: (1) particle-assisted membrane rupture, (2) particle translocation followed by membrane resealing, and (3) particle insertion into a metastable pore followed by membrane rupture. These results suggest a direct role of the nanoparticle in the endosomal escape, not envisioned in the proton sponge hypothesis. In all cases, sufficiently high membrane tension is required for the nucleation barriers to be surmountable on realistic time scales, suggesting that the osmotic pressure component of the proton sponge hypothesis is crucial for the successful endosomal escape of the nanoparticles. This conclusion is consistent with the theoretical work of Yang and May [14], which found that the nanoparticle alone would not lead to enough osmotic pressure to induce sufficient membrane tension, and that some excess free polymers are needed. Experimental studies revealed that the presence of these free polymers can increase the gene transfection efficiency by up to two orders of magnitude [43,44]. In what follows, we summarize our findings on the three nucleated pathways.

For particle-assisted membrane rupture, a key consideration is the membrane structure at the transition state, which is primarily controlled by the membrane tension. In particular, the membrane tension must be sufficiently high, so that the size of the critical nucleus (e.g. a solvophilic stalk) is on the order of the particle radius. Once this criterion is met, the charges on the particle should be enough to promote the adsorption onto and subsequent puncture of the membrane but not so much as to stabilize the pore. The particle solvophobicity is unimportant in this case, since rupture occurs before the particle has had significant interaction with the solvophobic tail region of the membrane.

In the case of particle translocation, increasing particle charge *increases* the barrier because the particle gains more favorable electrostatic interactions by adsorbing onto the surface of the membrane rather than inserting into a pore. In contrast, increasing particle solvophobicity *decreases* the barrier for translocation because the particle inserted into a pore can interact favorably with the lipid tails. Again, membrane tension is critical to reaching barriers surmountable on realistic time scales. With sufficient tension, the pore with a particle inserted into the center of the membrane becomes a metastable state on the MFEP to translocation. This state suggests—and indeed we find—another nucleated pathway from this metastable state: pore expansion, leading to rupture.

The mode of crossing the membrane bilayer depends on the membrane tension and the particle

properties. Here, we have considered particle radius, charge density and solvophobicity. Even within this set of parameters, we have not exhaustively explored the space for the most likely nucleation pathways. With the introduction of other types of interactions, for example specific ligand-receptor interactions [21] or different geometries [22], it should be possible that any of the pathways can become most favorable. The types of calculations illustrated in this work can be used to identify the optimal conditions for selecting a particular pathway.

Finally, the methodology developed in this work represents the most advanced theoretical technique for describing nucleation pathways in soft condensed matter systems that also include hard-particle degrees of freedom. We expect the method to be useful for studying a wide range of nucleation phenomena beyond membrane systems, for example, in nanoparticle polymer composites [29, 45, 46].

References

[1] N. Lewinski, V. Colvin, and R. Drezek, *Small* **4**, 26 (2008).

[2] R. Duncan, *Nat. Rev. Drug Discov.* **2**, 347 (2003).

[3] D. W. Pack, A. S. Hoffman, S. Pun, and P. S. Stayton, *Nat. Rev. Drug Discov.* **4**, 581 (2005).

[4] B. Alberts, A. Johnson, J. Lewis, M. Raff, K. Roberts, and P. Walter, *Molecular Biology of the Cell* (Garland Science, New York and Abingdon, 2007).

[5] J. Haensler and F. C. Szoka, *Bioconj. Chem.* **4**, 372 (1993).

[6] J. Behr, *Chimia*, **51**, 34 (1997).

[7] N. D. Sonawane, F. C. Szoka, and A. S. Verkman, *J. Biol. Chem.* **278**, 44826 (2003).

[8] L. Fournier and B. Joós, *Phys. Rev. E* **67**, 051908 (2003).

[9] V. Talanquer and D. Oxtoby, *J. Chem. Phys.* **118**, 872 (2003).

[10] T. Tolpekina, W. den Otter, and W. Briels, *J. Chem. Phys.* **121**, 12060 (2004).

[11] O. Farago and C. D. Santangelo, *J. Chem. Phys.* **122**, 044901 (2005).

[12] P. A. Boucher, B. Joós, M. J. Zuckermann, and L. Fournier, *Biophys. J.* **92**, 4344 (2007).

[13] C. L. Ting, D. Appelö, and Z.-G. Wang, *Phys. Rev. Lett.* **106**, 168101 (2011).

[14] S. Yang and S. May, *J. Phys. Chem.* **129**, 185105 (2008).

[15] V. V. Ginzburg and S. Balijepalli, *Nano Lett.* **7**, 3716 (2007).

[16] A. Alexeev, W. E. Uspal, and A. C. Balazs, *ACS Nano* **2**, 1117 (2008).

[17] Y. Li and N. Gu, *J. Phys. Chem. B* **114**, 2749 (2010).

[18] C. L. Ting and Z.-G. Wang, *Biophys. J.* **100**, 1288 (2011).

[19] R. C. Van Lehn and A. Alexander-Katz, *Soft Matter* **7**, 11392 (2011).

[20] H. Lee and R. G. Larson, *Molecules* **14**, 423 (2009).

[21] R. Vácha, F. J. Martinez-Veracoechea, and D. Frenkel, *Nano Lett.* **11**, 5391 (2011).

[22] K. Yang and Y. Q. Ma, *Nat. Nanotech.* **5**, 579 (2010).

[23] C. Dellago, P. G. Bolhuis, F. S. Csajka, and D. Chandler, *J. Phys. Chem.* **108**, 1964 (1998).

[24] P. G. Bolhuis, D. Chandler, C. Dellago, and P. L. Geissler, *Annu. Rev. Phys. Chem.* **53**, 291 (2002).

[25] X. Cheng, L. Lin, W. E, P. Zhang, and A.-C. Shi, *Phys. Rev. Lett.* **104**, 148301 (2010).

[26] G. H. Fredrickson, *The Equilibrium Theory of Inhomogeneous Polymers* (Oxford University Press, New York, 2005).

[27] W. E, W. Ren, and E. Vanden-Eijnden, *Phys. Rev. B* **66**, 052301 (2002).

[28] W. E, W. Ren, and E. Vanden-Eijnden, *J. Chem. Phys.* **126**, 164103 (2007).

[29] S. W. Sides, B. J. Kim, E. J. Kramer, and G. H. Fredrickson, *Phys. Rev. Lett.* **96**, 250601 (2006).

[30] M. W. Matsen and R. B. Thompson, *Macromolecules* **41**, 1853 (2008).

[31] K. Hong and J. Noolandi, *Macromolecules* **13**, 964 (1980).

[32] D. Needham and R. Nunn, *Biophys. J.* **58**, 997 (1990).

[33] H. Brockman, *Chem. Phys. Lipids* **73**, 57 (1994).

[34] N. M. Maurits and J. G. E. M. Fraaije, *J. Chem. Phys.* **107**, 5879 (1997).

[35] J. G. E. M. Fraaije, *J. Chem. Phys.* **99**, 9202 (1993).

[36] H. D. Ceniceros and G. H. Fredrickson, *Multiscale Model. Sim.* **2**, 452 (2004).

[37] X. He and F. Schmid, *Macromolecules* **39**, 2654 (2006).

[38] G. Crawford and J. Earnshaw, *Biophys. J.* **52**, 87 (1987).

[39] N. G. van Kampen, *Stochastic Processes in Physics and Chemistry* (Elsevier, New York, 1992).

[40] W. Pan, A. B. Kolomeisky, and P. G. Vekilov, *J. Chem. Phys.* **122**, 17905 (2005).

[41] F. Zhao, Y. Zhao, Y. Liu, X. L. Chang, C. Y. Chen, and Y. L. Zhao, *Small* **7**, 1322 (2011).

[42] A. J. Cann, *Principles of Molecular Virology* (Academic Press, 2001).

[43] S. Boeckle, K. von Gersdorff, S. van der Piepen, C. Culmsee, E. Wagner, and M. Ogris, *J. Gene Med.* **6**, 1102 (2004).

[44] Y. Yue, F. Jun, R. Deng, J. Cai, Y. Chen, M. C. M. Lin, H.-F. Kung, and C. Wu, *J. Control. Release* **155**, 67 (2011).

[45] R. B. Thompson, V. V. Ginzburg, M. W. Matsen, and A. C. Balazs, *Science* **292**, 2469 (2001).

[46] A. C. Balazs, T. Emrick, and T. P. Russell, *Science* **314**, 1107 (2006).

DISTRIBUTION:

1	MS 0359	D. Chavez, LDRD Office, 1911 (electronic copy)
1	MS 0899	Technical Library, 9536 (electronic copy)

Sandia National Laboratories